

Spatial Control of Coherent Anti-Stokes Emission with Height-Modulated Gold Zig-Zag Nanowires

Hyunmin Kim, David K. Taggart, Chengxiang Xiang, Reginald M. Penner, and Eric Olaf Potma*

Department of Chemistry, University of California, Irvine, California 92697-2025

Received April 28, 2008; Revised Manuscript Received June 13, 2008

ABSTRACT

Intrinsic coherent anti-Stokes emission is observed in lithographically patterned gold nanowires. Polarization dependent measurements reveal that the nanostructure's anti-Stokes response is polarized in the direction of the transverse surface plasmon resonance of the wire. We have used specially fabricated gold nanozigzag wires that are modulated in height between 20 and 80 nm to demonstrate tuning of the plasmon polarizability through control of wire height. Stronger anti-Stokes emission is shown to correlate with structures that support higher plasmon polarizability, underlining the primary role of the transverse plasmon resonance in the generation of anti-Stokes radiation from gold nanostructures. Our results also point out that a potential surface-enhanced coherent anti-Stokes Raman scattering (CARS) assay for detecting the vibrational response of surface-tethered molecules needs to include a mechanism for separating the molecular response from the strong intrinsic anti-Stokes emission of the metallic nanosubstrate.

The optical properties of metallic nanostructures are largely governed by the presence of surface plasmon resonances. The strong local fields associated with the surface plasmon resonances can enhance optical signatures that are otherwise too weak to detect. In particular, the strong local fields can lift the weak optical response of molecules tethered to the metal surface to detectable levels. Surface enhanced Raman scattering (SERS) is based on this effect.¹⁻⁴ With local fields of several orders of magnitude higher than the incident driving field, the SERS response is typically 10^6 higher compared with conventional spontaneous Raman scattering. Combined with electronic resonances in the molecule, the total signal enhancement is high enough to detect the Raman scattering from single molecules.^{5,6} Since the strength of the local fields crucially depends on the geometry of the nanosubstrate, a careful design of the metallic structure is required for optimizing the efficiency of SERS molecular detection assays.

Surface plasmon enhanced fields are also the candidates of choice for improving the nonlinear optical response from molecules. Surface enhanced coherent anti-Stokes Raman scattering (SE-CARS) is of particular interest because it offers a route for exploring the coherent vibrational response of molecules in very dilute samples. Initial SE-CARS measurements have indicated that enhancement of molecular optical nonlinearities can indeed be achieved at surfaces of noble metal nanostructures.⁷⁻⁹

So far, however, a straightforward implementation of a SE-CARS assay has not been demonstrated yet. An important hurdle in developing nanostructures suitable for SE-CARS is the intrinsic emission of the metal substrate. While the emissive response of the metal nanostructure is often negligible in SERS experiments, radiative contributions of the substrate itself are prominent under conditions of ultrafast laser irradiation.¹⁰⁻¹² The presence of surface plasmon resonances enhances coherent nonlinear signals such as second harmonic generation (SHG)^{13,14} and third harmonic generation (THG)¹⁵ of the metal substrate. In addition, the surface plasmon also enhances the two-photon absorption process in gold, which is coupled to a broad visible luminescence from the nanostructure.^{11,12,16,17} A first step toward the design of a reliable assay for surface-enhanced nonlinear coherent spectroscopy is to understand the intrinsic emission of the nanostructure under ultrafast illumination.

Coherent anti-Stokes scattering (CAS) signals have been observed from coupled pairs of gold nanospheres in near-field four-wave mixing experiments,¹⁸ indicating that plasmon resonances enable the generation of radiation at shifted frequencies when driven by two optical fields of different color simultaneously. Nonetheless, it is unclear how the coherent anti-Stokes emission scales with dimension and shape of the nanostructure, information that will be essential in potential SE-CARS experiments.

In this paper, we explore the intrinsic third order nonlinear optical response of scalable gold nanostructures through

* Corresponding author. E-mail: epotma@uci.edu.

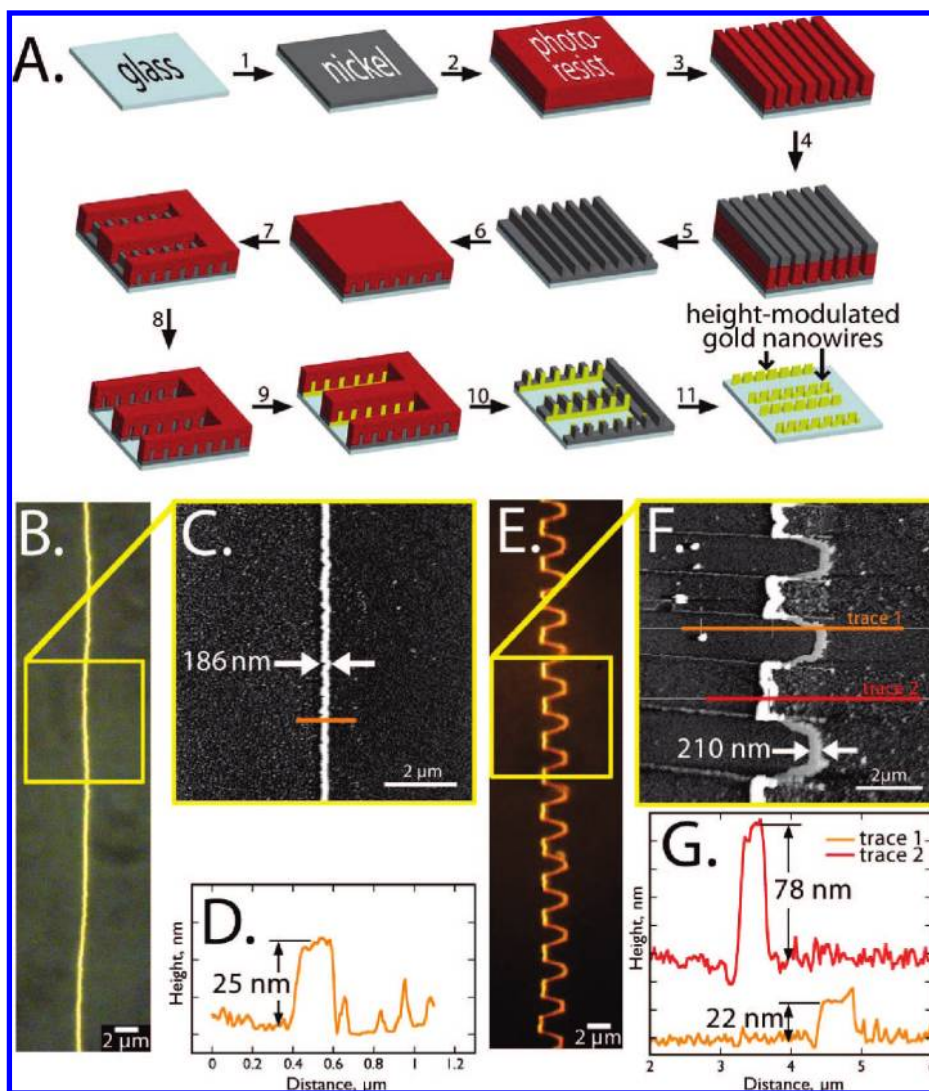


Figure 1. Fabrication and characterization of gold nanowires type I and type II. (A) Schematic of the fabrication method of height modulated nanowires (type II). (B) Dark-field transmission image of wire type I. (C) AFM image of wire type I, and cross-sectional profile (D) as measured with AFM. (E) Dark-field transmission image of wire type II, along with AFM image (F) and AFM cross-sectional profile (G).

coherent anti-Stokes radiation using far-field nonlinear microscopy. To enable precise dimension control, we have chosen gold nanowires as our model system. Two types of nanowires were examined: (type 1) flat gold nanowires with a defined height (25.3 nm) and width (186 nm) and (type 2) height modulated, zigzag nanowires. Both types of nanowires were prepared using lithographically patterned nanowire electrodeposition (LPNE), which produces nanowires having a rectangular cross section in which the wire height and width can be independently specified while the longitudinal axis of the wire can extend to several millimeters. This flexibility in nanowire fabrication not only allows us to study the wire's intrinsic anti-Stokes radiation as a function of aspect ratio but also allows us to control the intrinsic coherent anti-Stokes emission as a function of position by modulating the dimension of the wire. Nanowires have previously been shown to be excellent SERS substrates, emphasizing their potential use in an SE-CARS assay.¹⁹ The results in this work show that the ability to tune the third order polarizability of the wire through

dimension control adds additional degrees of flexibility to the design of reliable SE-CARS substrates.

Type 1 nanowires with lateral dimensions of 25.3×186 nm were prepared as previously described.²⁰ Type 2 nanowires were fabricated using a variant of the lithographically patterned nanowire electrodeposition (LPNE) shown schematically in Figure 1A. A description of the operations depicted there follows: (Step 1) Onto a cleaned glass microscope slide, a 20 nm nickel film (ESPI, 5N purity) was deposited by hot-filament evaporation ($0.5\text{--}1.0 \text{ \AA/s}$). (Step 2) A positive photoresist (PR, Shipley 1808) layer, $\approx 1 \mu\text{m}$ in thickness, was deposited by spin coating. This PR layer was soft-baked at $90 \text{ }^\circ\text{C}$ for 30 min. (Step 3) The sample was mounted in a mask alignment fixture (Newport Corporation, model 83210), and the PR was exposed (500 W for 1.2 s) through a quartz contact mask (Photo Sciences Inc.) using 365 nm illumination from a xenon arc lamp (Newport Corporation, model 69910). The exposed PR was developed (Shipley MF-351) for 25 s and rinsed with Millipore water. (Step 4) An additional 60 nm of Ni was thermally evaporated

as in step 1. (Step 5) The sample surface was vigorously rinsed with acetone to remove the PR and excess nickel, leaving a height-modulated Ni film having regions 80 nm in height and regions 20 nm in height. Now this height-modulated nickel layer was patterned, and a nanowire electrodeposited exactly as in the normal LPNE process to produce a height modulated nanowire mimicking the height profile of this nickel film. (Step 6) A PR layer was again deposited onto this nickel film as described in step 2. (Step 7) The PR was again exposed using a contact mask using the same conditions as specified in step 3 and the exposed PR was removed using developer. (Step 8) An undercut was then produced along the perimeter of the exposed regions by dissolving the exposed nickel in 0.8 M nitric acid for 8 min. The zigzag profile of the nanowires seen in Figure 1 is produced in this step because the thinner, 20 nm nickel regions of the nickel film dissolve more rapidly than the 80 nm regions. (Step 9) The electrochemical deposition of a gold nanowire was carried out by immersing the patterned and etched nickel film in a 100 mL, one compartment, three-electrode cell. Gold was deposited potentiostatically (Gamry, model G300) from an aqueous commercial gold-plating solution (Clean Earth Solutions, a 6 mM AuCl₃ solution) at -0.90 V for 200 s versus saturated calomel electrode (SCE). (Step 10) The surface was rinsed with Millipore water and then with acetone to remove the PR. (Step 11) The sacrificial nickel layer was removed by exposure to nitric acid for 15–30 min, exposing the height-modulated gold nanowires.

Figure 1B shows a dark-field transmission image of a type I wire. A scanning electron microscopy (AFM) reveals that the width of the average wire is about 185 nm, as shown in Figure 1C. The atomic force microscopy profile depicted in Figure 1D confirms the rectangular shape of the nanowire. A dark-field transmission image of a type II wire is given in Figure 1E. The AFM image in Figure 1F clearly shows the two distinct segments of the wire, whose height alternates between 78 and 22 nm (Figure 1G).

In the nonlinear imaging studies, the wires were visualized by raster-scanning the focal spot of a 1.15 NA water immersion lens across the wire in a laser-scanning microscope. The wires were illuminated by the focused light derived from two high-repetition rate 7 ps pulse trains generated by a mode-locked Nd:vanadate laser, producing the “Stokes” beam at 1064 nm, and a synchronously pumped optical parametric oscillator system, delivering the “pump” beam at 780 nm. The average beam power at the wire never exceeded 2 mW.

Figure 2A shows the optical transmission image of a grid of type I nanowires. Several distinct nonlinear processes were observed when the gold nanowires were subject to ultrafast illumination. Two-photon excited luminescence (TPEL) and second-harmonic generation were seen when the wires were illuminated with either pump (Figure 2B) or Stokes (Figure 2C) radiation. Much stronger signals were obtained when the collinear pump and Stokes beams were used simultaneously, as shown in Figure 2D. This enhancement is explained by the appearance of coherent anti-Stokes emission from the wire, as is evident from the single-wire emission

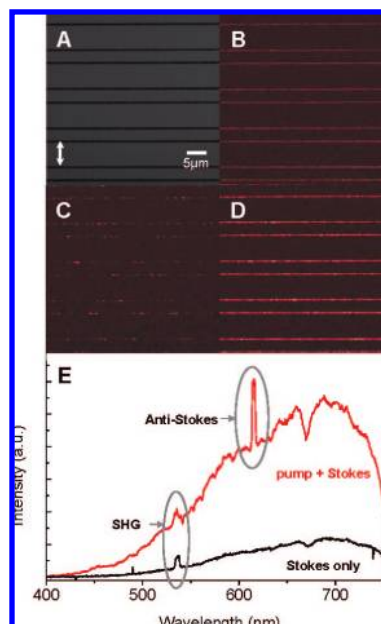


Figure 2. Nonlinear imaging of lithographically patterned nanowires. The infinitely extended rectangular parallelepiped gold nanowires have dimensions 25.3 nm (thickness) and 186 nm (width). (A) Transmission image. White arrows indicates incident beam polarization. (B) Two-photon excited luminescence from the pump. (C) Two-photon excited luminescence from the Stokes. (D) Total nonlinear signal when pump and Stokes are incident simultaneously. Pump (780 nm) was 0.2 mW and Stokes (1064 nm) was 0.8 mW. Nonlinear signal were detected through a 600 nm bandpass filter. (E) Total emission spectrum for Stokes only and combined pump and Stokes excitation.

spectrum in Figure 2E, where a clear anti-Stokes signal is identified in addition to the SHG response and the broad TPEL. The coherent anti-Stokes contribution to the signal can be easily determined by separately characterizing the TPEL background at the anti-Stokes wavelength.

The strong coherent and incoherent emission from the nanowire results from actively driving the structure’s surface plasmon mode, which is strongly resonant with the pump wavelength and weakly resonant with the Stokes beam. The enhanced local fields associated with the surface plasmon resonance promote the simultaneous absorption of two photons by the metal, exciting d electrons to the unoccupied sp band.^{11,12} The incoherent emission results from the electron–hole recombination at the Fermi level. Contrary to the luminescence, the coherent emission is independent of excitation of bulk metal states and is directly induced by the plasmon resonance enhanced third order polarization of the structure’s surface electron clouds.

To study the role of the surface plasmon in the coherent anti-Stokes emission process, we have examined the CAS signal as a function of polarization. Strongest anti-Stokes signals are seen when the beam polarization is aligned with the transverse axis of the wire, while negligible signal is observed when the beam polarization is oriented along the wire’s longitudinal axis. The CAS polarization dependence shows a $\sin^6 \theta$ dependence, where θ is the angle between the beam polarization and the longitudinal axis of the wire (Figure 3). This finding supports the notion that coherent

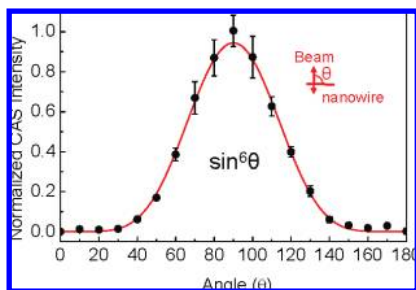


Figure 3. Polarization dependence of coherent anti-Stokes emission as a function of the angle θ between beam polarization and longitudinal axis of the wire. The fitted line follows a $\sin^6 \theta$ angular dependence. Excitation and detection conditions are identical as in Figure 2.

anti-Stokes emission is the result of a third-order nonlinear electronic polarization in the direction of the polarizability of the transverse plasmon resonance. We note that the TPEL polarization dependence exhibits the expected $\sin^4 \theta$ dependence (data not shown), emphasizing the different origin of the signal.

We next examine the nonlinear anti-Stokes signal strength as a function of nanowire geometry. In particular, the height of the wire is expected to strongly influence the relative polarizability of the plasmon resonance. To make a comparative study of the nanowire height possible, we have used the type II nanowires, which feature two separate heights incorporated in a single nanostructure. In this precisely controlled sample configuration, the relative anti-Stokes signal can be directly correlated to geometry-dependent surface plasmon properties.

A transmission image of the nanozigzags is shown in Figure 4A. The wire's height alternates between 20 and 80 nm every $\sim 2 \mu\text{m}$. The CAS image in Figure 4B reveals that the ratio between the lower and the higher parts of the wire is ~ 60 times, indicating that the polarizability of the plasmon resonance is much higher when the height is 20 nm. Note that virtually no TPEL was observed from the type II nanozigzags, as is evident from Figure 4D.

The height-dimension dependence of the CAS signal can be conveniently calculated with the lightning rod model.^{21,22} In this model, an estimate for the local field enhancement is determined as a function of the aspect ratio (width/height) of the nanostructure. Within the approximation that the rectangular nanowire cross section can be modeled as an ellipse, a simple analytical expression for the local field enhancement L is obtained.²¹ The results for the CAS enhancement are plotted as function of the height of the wire in Figure 4E. The calculated ratio between the CAS signal enhancement of the lower parts and that of the higher parts of the wire is about 125, which is within the same order of magnitude of what is found experimentally. The agreement between the predicted and the measured enhancement of the signal indicates that the CAS signal directly scales with the local field enhancement associated with the plasmon resonance.

In conclusion, we have shown that strong coherent anti-Stokes scattering can be detected from individual gold

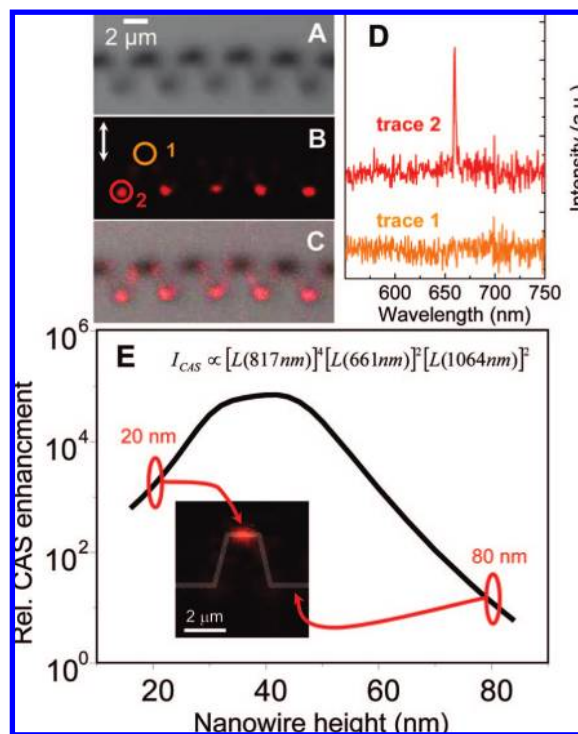


Figure 4. (A) Transmission image, (B) coherent anti-Stokes image, and (C) overlay image of nanozigzags. Emission spectra from the points 1 and 2 indicated in B are shown in D. Trace 2 is offset for clarity. (E) Calculated CAS enhancement as a function of nanowire height using the lightning rod model. Marked regions indicate the relevant heights of the nanozigzag structure. The local field enhancement factor L is calculated as in ref 21.

nanowires. The excitation polarization dependence indicates that the plasmon resonance is the primary source of intrinsic nonlinear anti-Stokes response of gold nanostructures. By optimizing the wire's geometry in terms of height, the surface plasmon polarizability was optimized for generating anti-Stokes radiation while two-photon excited luminescence contributions were strongly suppressed. In addition, the ability to precisely administer the nanostructure's dimensions allowed us to tune the coherent anti-Stokes emission spatially along the wire. Such forms of control will be crucial in tailoring the nonlinear optical properties of metallic nanostructures. While our results demonstrate that strong coherent anti-Stokes emission can be generated from metallic nanosubstrates, it is also clear that a potential SE-CARS assay for molecular analysis needs to incorporate a proper mechanism for isolating the CARS molecular response from the strong intrinsic anti-Stokes radiation of nanostructured substrates themselves.

Acknowledgment. We thank Professor Ara Apkarian for providing the CCD camera used in this study, and for helpful discussions. R.M.P. acknowledges the financial support of the NSF Grant CHE-0641169. E.O.P. is grateful for support received through the NSF-sponsored Chemical Bonding Center, Grant CHE-0533162, and acknowledges support from the American Chemical Society (PRF 46067-G6). The authors thank Travis Kruse for preparing the schematic shown in Figure 1A.

Supporting Information Available: Schematic diagram of microscope setup, CAS polarization dependence in gold

nanozigzags. This material is available free of charge via the Internet at <http://pubs.acs.org>.

References

- (1) Moskovits, M. "Surface-enhanced spectroscopy". *Rev. Mod. Phys.* **1985**, *57*, 783–826.
- (2) Kneipp, K.; Dasari, R. R.; Wang, Y. "Near-infrared surface-enhanced Raman scattering (NIR SERS) on colloidal silver and gold. *Appl. Spectrosc.* **1994**, *48*, 951–955.
- (3) Lee, P. C.; Meisel, D. "Absorption and surface-enhanced Raman of dyes on silver and gold sols. *J. Phys. Chem.* **1982**, *86*, 3391–3395.
- (4) Otto, A.; Mrozek, I.; Grabborn, H.; Akermann, A. "Surface-enhanced Raman scattering. *J. Phys.: Condens. Matter* **1992**, *4*, 1143–1212.
- (5) Nie, S.; Emory, S. R. "Probing single molecules and single nanoparticles by surface-enhanced Raman scattering". *Science* **1997**, *275*, 11021106.
- (6) Dieringer, J. A.; Lettan, R. B.; Scheidt, K. A.; Duyn, R. P. V. "A frequency-domain proof of single molecule surface-enhanced Raman spectroscopy. *J. Am. Chem. Soc.* **2007**, *129*, 16249–16256.
- (7) Ichimura, T.; Hayazawa, N.; Hashimoto, M.; Inouye, Y.; Kawata, S. "Local enhancement of coherent anti-Stokes Raman scattering by isolated gold nanoparticles". *J. Raman Spectrosc.* **2003**, *34*, 651–654.
- (8) Ichimura, T.; Hayazawa, N.; Hashimoto, M.; Inouye, Y.; Kawata, S. "Tip-enhanced coherent anti-Stokes Raman scattering for vibrational nanoimaging. *Phys. Rev. Lett.* **2004**, *92*, 220801.
- (9) Koo, T. W.; Chan, S.; Berlin, A. A. "Single-molecule detection of biomolecules by surface-enhanced coherent Raman scattering. *Opt. Lett.* **2005**, *30*, 1024.
- (10) Beversluis, M. R.; Bouhelier, A.; Novotny, L. "Continuum generation from single gold nanostructures through near-field mediated intraband transitions". *Phys. Rev. B* **2003**, *68*, 115433.
- (11) Boyd, G. T.; Yu, Z. H.; Shen, Y. R. "Photoinduced luminescence from the noble metals and its enhancement on roughened surfaces". *Phys. Rev. B* **1986**, *33*, 7923–7936.
- (12) Imura, K.; Nagahara, T.; Okamoto, H. "Near-field two-photon induced photoluminescence from single gold nanorods and imaging of plasmon modes. *J. Phys. Chem. B* **2005**, *109*, 13214–13220.
- (13) Antoine, R.; Brevet, P. F.; Girault, H. H.; Bethell, D.; Schiffrin, D. "Surface plasmon enhanced non-linear optical response of gold nanoparticles at the air-toluene interface". *Chem. Commun.* **1997**, *19*, 1901–1902.
- (14) Bouhelier, A.; Beversluis, M.; Hartschuh, A.; Novotny, L. "Near-field second-harmonic generation induced by local field enhancement. *Phys. Rev. Lett.* **2003**, *90*, 013903.
- (15) Lippitz, M.; Dijk, M. A. v.; Orrit, M. "Third-harmonic generation from single gold nanoparticles. *Nano Lett.* **2005**, *5*, 799–802.
- (16) Bouhelier, A.; Bachelot, R.; Lerondel, G.; Kostcheev, S.; Royer, P.; Wiederrecht, G. P. "Surface plasmon characteristics of tunable photoluminescence in single gold nanorods. *Phys. Rev. Lett.* **2005**, *95*, 267405–4.
- (17) Wang, H.; Huff, T. B.; Zweifel, D. A.; He, W.; Low, P. S.; Wei, A.; Cheng, J.-X. "In vitro and in vivo two-photon luminescence imaging of single gold nanorods". *Proc. Natl. Acad. Sci. U.S.A.* **2005**, *102*, 15752–15756.
- (18) Danckwerts, M.; Novotny, L. "Optical frequency mixing at coupled gold nanoparticles". *Phys. Rev. Lett.* **2007**, *98*, 026104, 026101–026104.
- (19) Billot, L.; Chapelle, M. L. d. l.; Grimault, A. S.; Barschiesi, V. A. D.; Bijeon, J. L.; Adam, P. M.; Royer, P. "Surface enhanced Raman scattering on gold nanowire arrays: evidence of strong multipolar surface plasmon resonance enhancement". *Chem. Phys. Lett.* **2006**, *422*, 303–307.
- (20) Menke, E. J.; Thompson, M. A.; Xiang, C.; Yang, L. C.; Penner, R. M. "Lithographically patterned nanowire electrodeposition". *Nature Mat.* **2006**, *5*, 914–919.
- (21) Boyd, G. T.; Rasing, T.; Leite, J. R. R.; Shen, Y. R. "Local-field enhancement on rough surfaces of metals, semimetals, and semiconductors with the use of optical second-harmonic generation". *Phys. Rev. B* **1984**, *30*, 519–525.
- (22) Liao, P. F.; Wokaun, A. "Lightning rod effect in surface enhanced Raman scattering". *J. Chem. Phys.* **1982**, *76*, 751–752.

NL801207A